AIAA JOURNAL
Vol. 39, No. 5, May 2001

Influence of Nonlinear Viscoelastic Material Characterization on Performance of Constrained Layer Damping Treatment

Farhan Gandhi*
Pennsylvania State University, University Park, Pennsylvania 16802

The influence of nonlinear viscoelastic material behavior on the performance of a passive constrained layer damping treatment is examined. For numerical simulations, a finite element model of a beam, simply supported at both ends, and with symmetric constrained layer damping treatments on the top and bottom surfaces, is considered. Results indicate that, if the viscoelastic material is relatively compliant, the damping provided by the treatment will decrease for increasing excitation levels, due primarily to the reduction in the viscoelastic material shear loss modulus. However, if the viscoelastic material is relatively stiff, the damping provided by the treatment will increase for increasing excitation levels, due primarily to increased shear in the viscoelastic layer associated with the decrease in its shear storage modulus. The benefits obtained by segmentation of the constrained layer damping treatment were seen to reduce substantially when the nonlinear behavior of the viscoelastic material was considered.

I. Introduction

OVER the past several years there has been considerable interest in the use of constrained layer damping treatments for structural vibration reduction and damping augmentation. Such damping treatments typically comprise a viscoelastic layer bonded to a host structure and covered by a relatively stiff constraining layer. As shown in Fig. 1, when the host structure undergoes deformation, the viscoelastic layer will shear and dissipate energy, thereby introducing damping into the system and attenuating vibration. The constraining layer in the damping treatment can be either passive or active. In a passive constrained layer (PCL) damping treatment, the purpose of the stiff constraining layer was simply to maximize the shear in the viscoelastic layer. An active constrained layer (ACL) damping treatment takes this concept further. By the introduction of a constraining layer made of an active material (such as a piezoelectric material), it is possible to further increase the shear in the viscoelastic layer by active elongation or shrinkage of the constraining layer over appropriate portions of the vibration cycle and, thereby, introduce additional damping. Further, the forces exerted on the structure by the piezoelectric layer can produce some additional vibration reduction through pure active control action. In recent years, several researchers have conducted both numerical as well as experimental investigations of the behavior of ACL damping treatments.[1–8]

In most of these studies, very flexible beams and plates are considered. The viscoelastic material used in the treatment usually comprises a layer of damping tape (for example, the type manufactured by 3M), whose shear modulus is relatively low. Whereas a low shear modulus viscoelastic material may be appropriate for relatively flexible structures, it would be ineffective if the constrained layer damping treatment were to be applied to relatively stiff structures such as buildings, bridges, tanks, and submarines. If PCL or ACL damping treatments are applied to such large and heavy structures, the viscoelastic material in the treatment would be required to have a considerably higher shear modulus, and elastomers such as silicone- or carbon-filled rubber might well be the material of choice. Such elastomers are used extensively in the production of heavy-duty commercial damping devices by manufacturers such as Lord Corporation and Paulstra. However, the behavior of these elastomeric materials is known to be nonlinearly dependent on the shear strain amplitude.[9–14] Figure 2 shows a reduction in both storage modulus G' (a measure of the shear stiffness) and loss modulus G'' (a measure of the damping capacity) of a typical elastomer, with increasing strain amplitude. Both the PCL and ACL concepts are based on the premise that increased shear strain levels in the viscoelastic layer (relative to the overall system deformations) would yield increased damping. Although this would generally be true for a linear viscoelastic material, it may not necessarily hold for a nonlinear viscoelastic material. For example, the decrease in the loss modulus with increasing shear strain amplitude could possibly cause a reduction in the damping. The present study seeks to investigate, in detail, the effects of the nonlinear viscoelastic material behavior (its amplitude-dependent storage and loss modulus) on the performance of PCL damping treatments. Both continuous and segmented treatments are considered.

Received 19 October 1999; revision received 23 July 2000; accepted for publication 23 July 2000.

*Assistant Professor, Department of Aerospace Engineering, 233 Hammond Building. Member AIAA.

II. Analytical Model and Solution Scheme

To examine the influence of nonlinear viscoelastic material characterization on constrained layer damping treatment performance, an elastic beam simply supported at both ends, with the treatment applied symmetrically on the upper and lower surfaces, is considered. The structure is discretized spatially using the finite element method (schematic shown in Fig. 3), with the development of the finite element equations of motion described in Sec. II.A. The nonlinear viscoelastic material behavior is represented by using an amplitude-dependent storage and loss modulus as indicated in Fig. 2. Although such a frequency-domain characterization of the nonlinear viscoelastic material behavior would not allow prediction of certain complex phenomena (for example, limit-cycle oscillations), it provides a good approximation of the change (either an increase or decrease) in damping that could be expected as compared to that available from a linear viscoelastic layer. Additionally, because such a frequency-domain characterization using complex modulus is routinely used for linear viscoelastic constrained layer damping treatments, it is very convenient for comparison. Section II.B describes the procedure used to calculate the damping.

A. Equations of Motion

1. Kinematics of Deformation

Figure 4 shows a section of the beam in the deformed configuration (where $\partial w_0/\partial x$ is the slope and γ is the shear angle in the viscoelastic layer) and can be used to obtain expressions for the axial displacements in the individual layers. The axial displacement in the base beam is

$$u^b = -z\frac{\partial w_0}{\partial x} \tag{1}$$

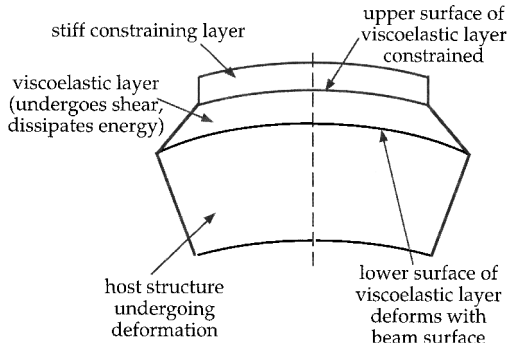

Fig. 1 Schematic of constrained layer damping concept.

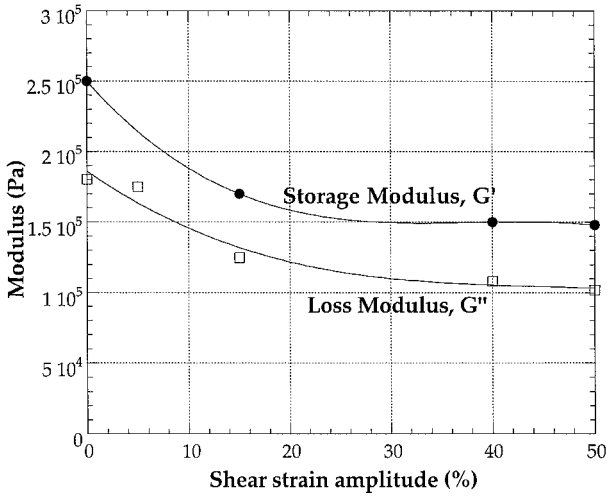

Fig. 2 Variation of viscoelastic material storage and loss modulus vs shear strain amplitude.

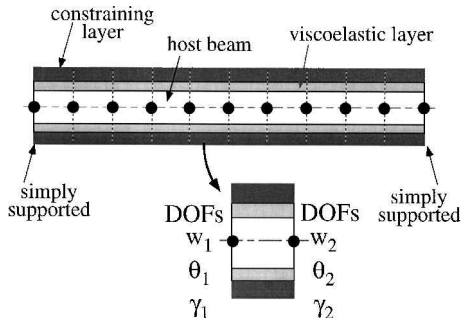

Fig. 3 Finite element discretization of beam with constrained layer damping concept.

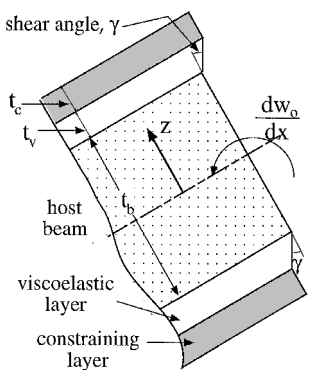

Fig. 4 Kinematics of deformation.

Axial displacements in the top and bottom viscoelastic layers, respectively, are

$$u^{vt} = -z\frac{\partial w_0}{\partial x} + \left(z - \frac{t_b}{2}\right)\gamma, \qquad u^{vb} = -z\frac{\partial w_0}{\partial x} + \left(z + \frac{t_b}{2}\right)\gamma \tag{2}$$

and the axial displacements in the top and bottom constraining layers, respectively, are

$$u^{ct} = -z\frac{\partial w_0}{\partial x} + t_v\gamma, \qquad u^{cb} = -z\frac{\partial w_0}{\partial x} - t_v\gamma \tag{3}$$

2. Strains in the Individual Layers

The normal strains in the individual layers can then be obtained as

$$\varepsilon_{xx}^{b} = -z\frac{\partial^2 w_0}{\partial x^2} \tag{4}$$

in the base beam,

$$\varepsilon_{xx}^{vt} = -z\frac{\partial^2 w_0}{\partial x^2} + \left(z - \frac{t_b}{2}\right)\frac{\partial \gamma}{\partial x}$$

$$\varepsilon_{xx}^{vb} = -z\frac{\partial^2 w_0}{\partial x^2} + \left(z + \frac{t_b}{2}\right)\frac{\partial \gamma}{\partial x} \tag{5}$$

in the top and bottom viscoelastic layers, respectively, and

$$\varepsilon_{xx}^{ct} = -z\frac{\partial^2 w_0}{\partial x^2} + t_v\frac{\partial \gamma}{\partial x}, \qquad \varepsilon_{xx}^{cb} = -z\frac{\partial^2 w_0}{\partial x^2} - t_v\frac{\partial \gamma}{\partial x} \tag{6}$$

in the top and bottom constraining layers, respectively. The transverse shear strain ε_{zx} is zero for the base beam and the constraining layers. For both upper and lower viscoelastic layers, $\varepsilon_{zx} = \gamma$.

3. Strain Energy Variation

The variation in strain energy δU has contributions due to flexural deformations and shear deformations and can be written as

$$\delta U = \int_{\text{volume}} (\delta\varepsilon_{xx}\sigma_{xx} + \delta\varepsilon_{xz}\sigma_{xz})\,\mathrm{d}V$$

$$= \int_0^L \left\{ \int_{\text{cross section}} \delta\varepsilon_{xx} E(z)\varepsilon_{xx} b\,\mathrm{d}z \right.$$

$$\left. + \int_{\text{cross section}} \delta\varepsilon_{zx} G_s^* \varepsilon_{zx} b\,\mathrm{d}z \right\} \mathrm{d}x \tag{7}$$

In Eq. (7) Young's modulus E varies from layer to layer (E_b for the beam, E_v for the viscoelastic material, and E_c for the constraining layer), and the viscoelastic layers alone contribute to the shear strain energy variations ($G^* = G' + jG''$ is the complex shear modulus, whose components vary with shear strain amplitude as indicated in Fig. 2). Introducing the expressions for strains in the various layers [Eqs. (4–6)] into Eq. (7) and evaluating the integrals over the cross-section yield

$$\delta U = \int_0^L \begin{bmatrix} \dfrac{\partial^2 \delta w_0}{\partial x^2} & \dfrac{\partial \delta\gamma}{\partial x} \end{bmatrix} \begin{bmatrix} C_{22} & C_{23} \\ C_{23} & C_{33} \end{bmatrix} \begin{Bmatrix} \dfrac{\partial^2 w_0}{\partial x^2} \\ \dfrac{\partial \gamma}{\partial x} \end{Bmatrix} \mathrm{d}x$$

$$+ \int_0^L \delta\gamma \left[2G_s^* b t_v\right]\gamma\,\mathrm{d}x \tag{8}$$

where

$$C_{22} = \frac{E_b b t_b^3}{12} + \frac{2E_v b}{3}\left[\left(\frac{t_b}{2} + t_v\right)^3 - \left(\frac{t_b}{2}\right)^3\right]$$

$$+ \frac{2E_c b}{3}\left[\left(\frac{t_b}{2} + t_v + t_c\right)^3 - \left(\frac{t_b}{2} + t_v\right)^3\right]$$

$$C_{23} = 2E_v b\left[-\frac{1}{3}\left\{\left(\frac{t_b}{2}+t_v\right)^3-\left(\frac{t_b}{2}\right)^3\right\}+\frac{t_b}{4}\left\{\left(\frac{t_b}{2}+t_v\right)^2-\left(\frac{t_b}{2}\right)^2\right\}\right]-E_c b t_v\left[\left(\frac{t_b}{2}+t_v+t_c\right)^2-\left(\frac{t_b}{2}+t_v\right)^2\right]$$

$$C_{33} = \frac{2E_v b t_v^3}{3}+2E_c b t_v^2 t_c \tag{9}$$

4. Kinetic Energy Variation

The variation in kinetic energy δT can be written as

$$\delta T = \int_0^L m\delta\dot{w}_0\dot{w}_0\,\mathrm{d}x+\int_0^L\left\{\int_{\text{cross section}}\varsigma(z)b\delta\dot{u}\dot{u}\,\mathrm{d}z\right\}\mathrm{d}x \tag{10}$$

The first term and second term, respectively, represent kinetic energy variation due to transverse motion, w_0, and longitudinal motion, u. Differentiating Eqs. (1–3) with respect to time to obtain the axial velocities in the individual layers and evaluating the integral over the cross section yields

$$\delta T = \int_0^L \delta\dot{w}_0 m\dot{w}_0\,\mathrm{d}x+\int_0^L\begin{bmatrix}\dfrac{\partial\delta\dot{w}_0}{\partial x} & \delta\dot{\gamma}\end{bmatrix}\begin{bmatrix}\tau_{22} & \tau_{23}\\ \tau_{23} & \tau_{33}\end{bmatrix}\times\begin{Bmatrix}\dfrac{\partial\dot{w}_0}{\partial x}\\ \dot{\gamma}\end{Bmatrix}\mathrm{d}x \tag{11}$$

where

$$\tau_{22} = \varsigma_b b\frac{t_b^3}{12}+\varsigma_v b\frac{2}{3}\left[\left(\frac{t_b}{2}+t_v\right)^3-\left(\frac{t_b}{2}\right)^3\right]+\varsigma_c b\frac{2}{3}\left[\left(\frac{t_b}{2}+t_v+t_c\right)^3-\left(\frac{t_b}{2}+t_v\right)^3\right]$$

$$\tau_{23} = -\varsigma_v b\frac{2}{3}\left[\left(\frac{t_b}{2}+t_v\right)^3-\left(\frac{t_b}{2}\right)^3\right]+\varsigma_v b\frac{t_b}{2}\left[\left(\frac{t_b}{2}+t_v\right)^2-\left(\frac{t_b}{2}\right)^2\right]-\varsigma_c b t_v\left[\left(\frac{t_b}{2}+t_v+t_c\right)^2-\left(\frac{t_b}{2}+t_v\right)^2\right]$$

$$\tau_{33} = \varsigma_v b\frac{2}{3}\left[\left(\frac{t_b}{2}+t_v\right)^3-\left(\frac{t_b}{2}\right)^3\right]-\varsigma_v b t_b\left[\left(\frac{t_b}{2}+t_v\right)^2-\left(\frac{t_b}{2}\right)^2\right]+\varsigma_v b\frac{t_b^2}{2}t_v+\varsigma_c b t_v^2 t_c \tag{12}$$

where ς_b, ς_v, and ς_c are the mass densities of the base beam, viscoelastic layer, and constraining layer, respectively.

5. Finite Element Discretiztion

The equations of motion are obtained by using expressions for strain energy variation [Eq. (8)] and kinetic energy variation [Eq. (11)] in the Hamilton's principle and by discretizing the structure using the finite element method (Fig. 3). Over the length of any individual element, the transverse displacement w_0 and the shear angle γ are assumed to vary as follows:

$$w_0 = N_{w_1}w_1+N_{\theta_1}\theta_1+N_{w_2}w_2+N_{\theta_2}\theta_2,\qquad \gamma = N_1\gamma_1+N_2\gamma_2 \tag{13}$$

where w_1 and θ_1 are the transverse displacement and slope at the left end node of the element, w_2 and θ_2 are corresponding values at the right end, and γ_1 and γ_2 are the shear angles at the left and right ends of the element, respectively. The shape functions in Eq. (13) are

$$\begin{bmatrix}N_{w_1} & N_{\theta_1} & N_{w_2} & N_{\theta_2}\end{bmatrix} = \begin{bmatrix}(1-3\xi^2+2\xi^3) & (-\xi+2\xi^2-\xi^3)l & (3\xi^2-2\xi^3) & (\xi^2-\xi^3)l\end{bmatrix}$$

$$\begin{bmatrix}N_1 & N_2\end{bmatrix} = \begin{bmatrix}(1-\xi) & \xi\end{bmatrix} \tag{14}$$

where ξ is the nondimensional local coordinate within the element ($0<\xi<1$) and l is the element length. When the element degree-of-freedom vector is denoted as $\{\boldsymbol{q}\} = \lfloor w_1\ \theta_1\ \gamma_1\ w_2\ \theta_2\ \gamma_2\rfloor^T$, from Eq. (13),

$$\begin{Bmatrix}\dfrac{\partial^2 w_0}{\partial x^2}\\ \dfrac{\partial\gamma}{\partial x}\end{Bmatrix} = [B_1]\{\boldsymbol{q}\}$$

$$[B_1] = \begin{bmatrix}\dfrac{1}{l^2}N''_{w_1} & \dfrac{1}{l^2}N''_{\theta_1} & 0 & \dfrac{1}{l^2}N''_{w_2} & \dfrac{1}{l^2}N''_{\theta_2} & 0\\ 0 & 0 & \dfrac{1}{l}N'_1 & 0 & 0 & \dfrac{1}{l}N'_2\end{bmatrix} \tag{15a}$$

$$\gamma = [B_2]\{\boldsymbol{q}\},\qquad [B_2] = [0\quad 0\quad N_1\quad 0\quad 0\quad N_2] \tag{15b}$$

where the derivatives of shape functions in Eq. (15a) are with respect to ξ. Introducing Eqs. (15) into Eq. (8) and integrating along the element length yield the 6×6 element stiffness matrix:

$$K = \int_0^1 [B_1]^T\begin{bmatrix}C_{22} & C_{23}\\ C_{23} & C_{33}\end{bmatrix}[B_1]l\,\mathrm{d}\xi+\int_0^1[B_2]^T\left[2G_s^* b t_v\right][B_2]l\,\mathrm{d}\xi$$

$$= \begin{bmatrix}
C_{22}\left(\frac{12}{l^3}\right) & C_{22}\left(-\frac{6}{l^2}\right) & 0 & C_{22}\left(-\frac{12}{l^3}\right) & C_{22}\left(-\frac{6}{l^2}\right) & 0\\
 & C_{22}\left(\frac{4}{l}\right) & -\frac{C_{23}}{l} & C_{22}\left(\frac{6}{l^2}\right) & C_{22}\left(\frac{2}{l}\right) & \frac{C_{23}}{l}\\
 & & \frac{C_{33}}{l}+\frac{2G_s^* b t_v l}{3} & 0 & \frac{C_{23}}{l} & -\frac{C_{33}}{l}+\frac{G_s^* b t_v l}{3}\\
 & & & C_{22}\left(\frac{12}{l^3}\right) & C_{22}\left(\frac{6}{l^2}\right) & 0\\
 & & & & C_{22}\left(\frac{4}{l}\right) & -\frac{C_{23}}{l}\\
 & & & & & \frac{C_{33}}{l}+\frac{2G_s^* b t_v l}{3}
\end{bmatrix} \tag{16}$$

From Eq. (13), the following expressions can also be obtained:

$$\dot{w} = [B_3]\{\dot{\boldsymbol{q}}\}, \qquad [B_3] = \begin{bmatrix} N_{w_1} & N_{\theta_1} & 0 & N_{w_2} & N_{\theta_2} & 0 \end{bmatrix} \tag{17a}$$

$$\begin{Bmatrix} \dfrac{\partial \dot{w}_0}{\partial x} \\ \dot{\gamma} \end{Bmatrix} = [B_4]\{\dot{\boldsymbol{q}}\}$$

$$[B_4] = \begin{bmatrix} \dfrac{1}{l}N'_{w_1} & \dfrac{1}{l}N'_{\theta_1} & 0 & \dfrac{1}{l}N'_{w_2} & \dfrac{1}{l}N'_{\theta_2} & 0 \\ 0 & 0 & N_1 & 0 & 0 & N_2 \end{bmatrix} \tag{17b}$$

Introducing Eqs. (17) into Eq. (11) and integrating along the element length yield the 6×6 element mass matrix:

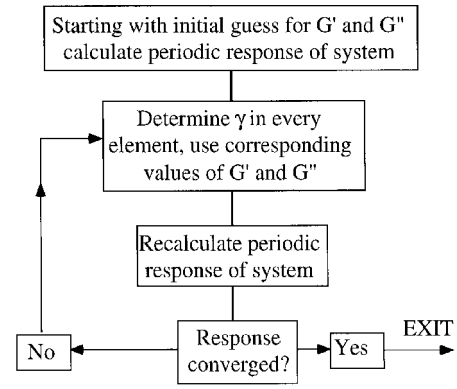

Fig. 5 Flowchart for iterative calculation of nonlinear response.

$$M = \int_0^1 [B_3]^T [m][B_3] l \, d\xi + \int_0^1 [B_4]^T \begin{bmatrix} \tau_{22} & \tau_{23} \\ \tau_{23} & \tau_{33} \end{bmatrix} [B_4] l \, d\xi$$

$$= \begin{bmatrix} \dfrac{156ml}{420} + \dfrac{36\tau_{22}}{30l} & -\dfrac{22ml^2}{420} - \dfrac{3\tau_{22}}{30} & -\dfrac{\tau_{23}}{2} & \dfrac{54ml}{420} - \dfrac{36\tau_{22}}{30l} & \dfrac{13ml^2}{420} - \dfrac{3\tau_{22}}{30} & -\dfrac{\tau_{23}}{2} \\ & \dfrac{4ml^3}{420} + \dfrac{4l\tau_{22}}{30} & -\dfrac{l\tau_{23}}{12} & -\dfrac{13ml^2}{420} + \dfrac{3\tau_{22}}{30} & -\dfrac{3ml^3}{420} - \dfrac{l\tau_{22}}{30} & \dfrac{l\tau_{23}}{12} \\ & & \dfrac{l\tau_{33}}{3} & \dfrac{\tau_{23}}{2} & \dfrac{l\tau_{23}}{12} & \dfrac{l\tau_{33}}{6} \\ & & & \dfrac{156ml}{420} + \dfrac{36\tau_{22}}{30l} & \dfrac{22ml^2}{420} + \dfrac{3\tau_{22}}{30} & \dfrac{\tau_{23}}{2} \\ & & & & \dfrac{4ml^3}{420} + \dfrac{4l\tau_{22}}{30} & -\dfrac{l\tau_{23}}{12} \\ & & & & & \dfrac{l\tau_{33}}{3} \end{bmatrix} \tag{18}$$

The element stiffness and mass matrices can be assembled to produce the global stiffness and mass matrices. After application of global geometric boundary conditions, the system equations of motion can be written as

$$M_G \ddot{\boldsymbol{q}}_G + K_G \boldsymbol{q}_G = \boldsymbol{F}_G \tag{19}$$

Note that $\boldsymbol{F}_G$ is the external load vector and that the global stiffness matrix is a complex matrix, $K_G = K'_G + jK''_G$ [because $G^* = G' + jG''$ in Eq. (16)].

B. Solutions of Equations of Motion and Damping Calculation

The system is subjected to a transverse sinusoidal excitation force at the midpoint. When an initial guess for the viscoelastic material storage and loss modulus is used, the harmonic balance method is used to calculate the system periodic response to the excitation force. With an estimate of the shear distribution along the length of the viscoelastic layer now available, updated values of storage and loss modulus are used for the different elements, and the response to the excitation force is recalculated. This process is continued iteratively until a converged nonlinear response is determined (Fig. 5). The process is then repeated over a range of different excitation frequencies, to obtain a frequency-response function for a given excitation load amplitude. Qualitatively, the frequency-response function appears fairly similar to that of a linear system (no clearly discernible evidence of softening behavior of jump phenomena), and the half-power bandwidth method is then used to estimate the equivalent damping ratio. Because the half-power bandwidth method is rigorously applicable to linear systems, the approach used here for damping calculation is an approximation. However, it is an effective approach that has also been used by other researchers examining the damping characteristics of complex nonlinear systems (for example, Ref. 15). The frequency-response function is then obtained for a number of different excitation amplitudes, to study the impact of the nonlinear viscoelastic behavior on the performance of the constrained layer damping treatment.

Note that the system has to be discretized into a large number of elements even when damping is only considered in the fundamental mode. This is because the shear strain varies significantly along the length of the treatment (assuming large values near the free edges and reduced values between). Because the viscoelastic material storage and loss modulus are strongly dependent on the shear strain amplitude, if the variation of the shear strain along the treatment length is not predicted accurately, that would compromise any study seeking to examine the effect of material nonlinearity on the performance of the treatment.

III. Results and Discussion

The damping in the first bending mode is numerically examined for a beam, simply supported at both ends, with PCL damping treatment extending over the entire length of the top and bottom surfaces. The material parameters used in the simulation are provided in Table 1 and the geometric parameters in Table 2. Two specific configurations are considered in the study. The differences between these two configurations are in the length of the beam and the thickness and shear modulus of the viscoelastic layer. For the continuous treatments considered in Secs. III.A and III.B, the beam is discretized into 10 elements along its length. For the segmented treatment in Sec. III.C, 20 elements are used because the shear strain variations along the treatment length are much more significant (details given in Sec. III.C).

A. Configuration 1

Figure 6 shows frequency-response functions for increasing amplitudes P_0 of the sinusoidal excitation force. For larger values of

Table 1 Material properties used in finite element simulation[a]

Property	Value
Young's modulus, N/m^2	
Beam	7.1×10^{10}
Constraining layer	6.49×10^{10}
Mass density, kg/m^3	
Beam	2700
Constraining layer	7600
Viscoelastic layer	1250

[a]Viscoelastic material storage and loss modulus for configuration 1 is provided in Fig. 2. Values for configuration 2 are larger by a factor of 20.

Table 2 Geometric properties used in finite element simulation

Property	Configuration 1	Configuration 2
Thickness, m		
Beam	4.0×10^{-3}	4.0×10^{-3}
Viscoelastic layer	1.0×10^{-3}	0.5×10^{-3}
Constraining layer	1.0×10^{-3}	1.0×10^{-3}
Length, m	300×10^{-3}	500×10^{-3}
Width, m	20.0×10^{-3}	20.0×10^{-3}

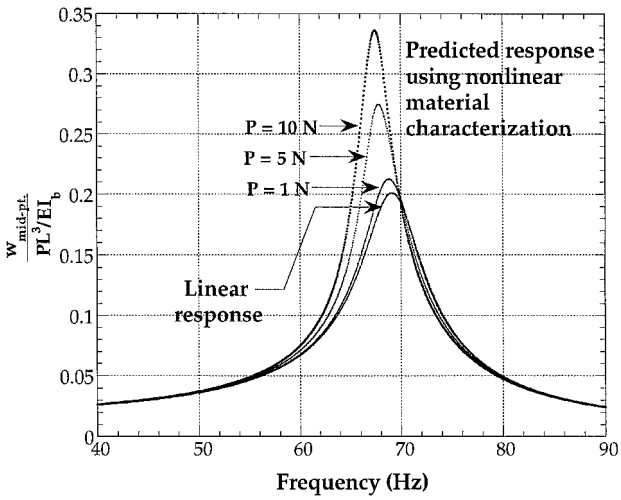

Fig. 6 Normalized frequency-response function for different excitation levels (configuration 1).

P_0, the normalized peak resonant response is seen to increase, which implies that there is less vibration attenuation and reduced damping will be available.

Figure 7a shows the variation in damping ratio vs increasing resonant response amplitude (due to increasing loading levels, P_0). When the viscoelastic material is assumed to be linear, the predicted damping in the fundamental mode is about 4.33% critical. When variation in storage modulus G' and loss modulus G'' vs amplitude is considered, the damping is seen to decrease for increasing excitation levels. This is consistent with the observations of Fig. 6. To develop a clearer physical understanding, individual variations of G' and G'' were also considered. Figure 7a indicates that, if variation in G'' alone is considered (G' constant), the decrease in damping ratio would be even larger. Conversely, if variation in G' alone is considered (G'' constant), the damping ratio would actually increase slightly with increasing excitation levels. This increase in damping can be attributed to increases in shear strain levels in the viscoelastic layer associated with the softening of the viscoelastic material at higher excitation levels (see Fig. 2). Thus, for larger excitation levels, the softening of the viscoelastic material (reduction in G') produces an increase in damping, whereas the reduction in the loss modulus G'' produces a decrease in damping. The net change in damping level due to variations in both G' and G'' is a combination of these two individual effects. For configuration 1, the reduction in damping

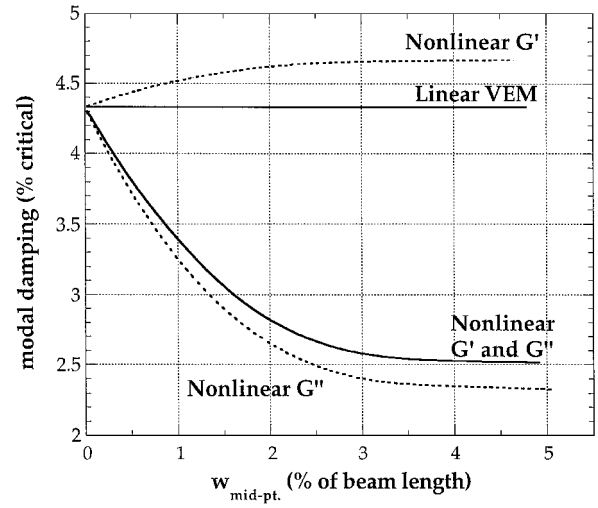

Fig. 7a Modal damping variation as a function of excitation level (configuration 1).

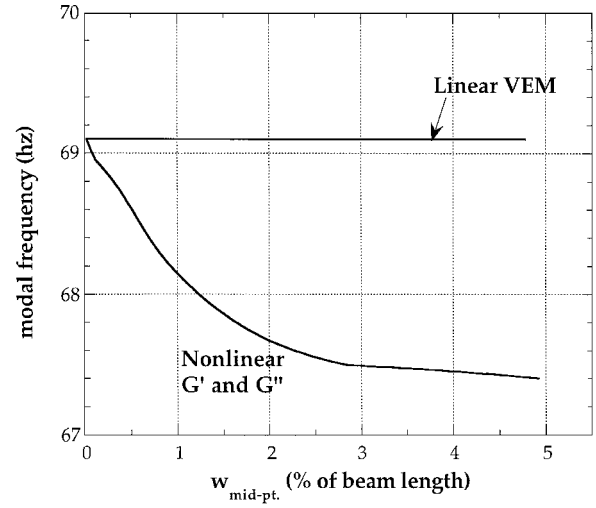

Fig. 7b Modal frequency variation as a function of excitation level (configuration 1).

due to a decrease in G'' is much more dominant and produces the net reduction seen in damping ratio. Note that the significant reduction in damping seen in Fig. 7a due to viscoelastic material nonlinearity was obtained for a maximum beam transverse displacement of no greater than 5% of the beam length (small enough that geometric nonlinearities would be insignificant). Figure 7b shows the variation in natural frequency, as a function of excitation levels. Although a reduction in natural frequency is seen due to the decrease in G' with excitation amplitude, the actual magnitude of this reduction is relatively insignificant.

Figures 8a and 8b show the variation in shear strain along the length of the constrained layer damping treatment when the system is driven at its fundamental frequency, for forcing amplitudes of $P_0 = 1$ N and $P_0 = 10$ N, respectively. For $P_0 = 1$ N (Fig. 8a), it is seen that the shear strain level is close to that predicted for a linear viscoelastic material (constant G' and G''). However, for $P_0 = 10$ N (Fig. 8b), the shear strain levels are considerably higher than those predicted for a linear viscoelastic material. The increase in shear strain, relative to that of a linear viscoelastic damping layer, is associated with the increased overall response amplitude at resonance, due to reduced system damping.

B. Configuration 2

Figure 9 shows the variation in damping ratio vs increasing resonant response amplitude for the configuration 2. As compared to configuration 1 (see Tables 1 and 2), the beam is longer, the viscoelastic layer thickness is reduced by one-half, and the viscoelastic

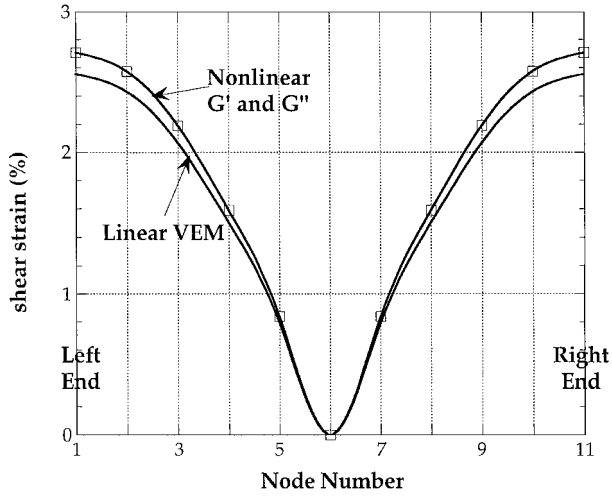

Fig. 8a Variation of shear strain along treatment length for $P_0 = 1$ N (configuration 1).

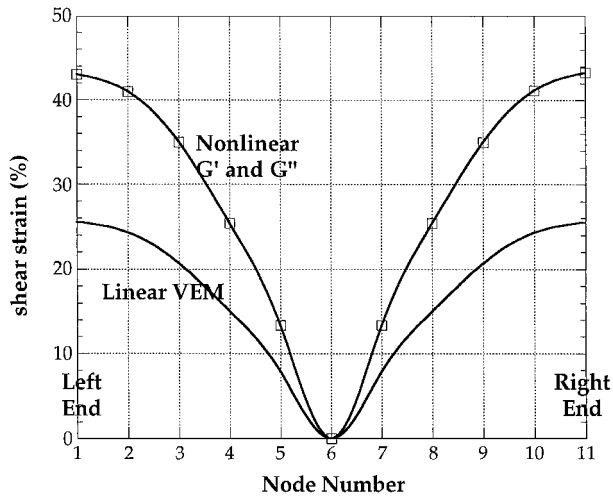

Fig. 8b Variation of shear strain along treatment length for $P_0 = 10$ N (configuration 1).

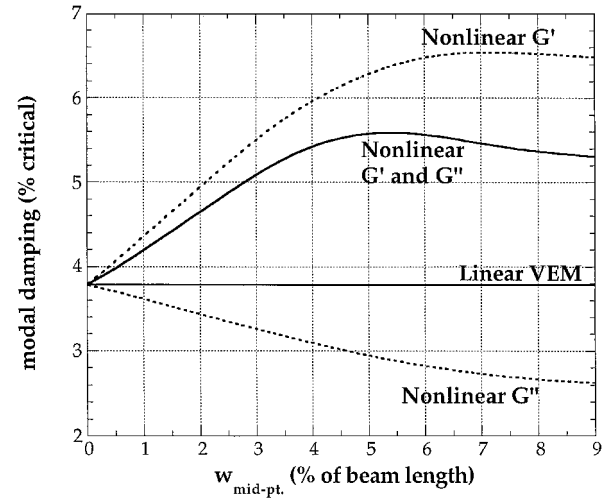

Fig. 9 Modal damping variation as a function of excitation level (configuration 2).

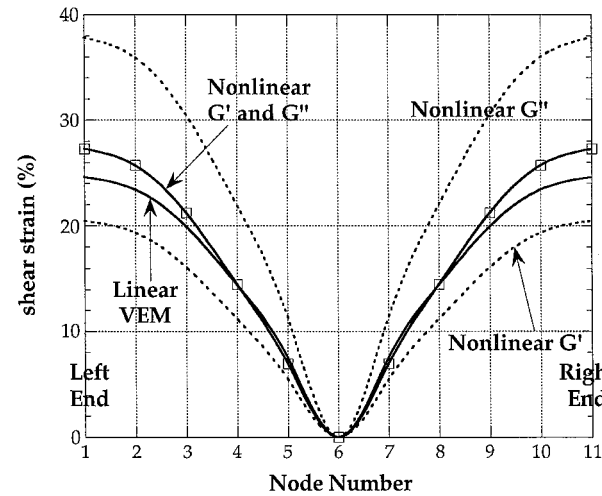

Fig. 10 Variation of shear strain along treatment length for $P_0 = 30$ N (configuration 2).

material shear modulus is increased by a factor of 20 (while retaining the same variation with strain amplitude shown in Fig. 2). For this system, if the viscoelastic material is assumed to be linear, the predicted damping in fundamental mode is 3.78%. When variation in G' and G'' with strain amplitude is considered, an increase in damping is observed for increasing excitation levels. This is in contrast to the results for configuration 1 (Fig. 7a), where the damping was seen to decrease for increasing excitation levels. Individual variations of G' and G'' were again considered for configuration 2. As was the case for configuration 1, Fig. 9 indicates that variation in G'' alone (G' constant) produces a decrease in damping, whereas variation in G' alone (G'' constant) produces an increase in damping. However, as compared to Fig. 7a (configuration 1), it is seen in Fig. 9 that the increase in damping due to the softening of the viscoelastic material is much more significant and is responsible for producing a net damping increase when variations in both G' and G'' are considered. Note that a relatively compliant viscoelastic material was used in configuration 1. This allowed the viscoelastic layer to undergo a fair amount of shear, and further softening did not have a dramatic influence. On the other hand, a relatively stiff viscoelastic material was used in configuration 2, which allowed smaller amounts of shear and energy dissipation. In this case, the softening of the viscoelastic material allowed a significant increase in shear and produced more damping.

Figure 10 shows the variation in shear strain along the length of the constrained layer damping treatment when the system is driven at its fundamental frequency, with $P_0 = 30$ N. When variation in G' alone is considered (G'' constant), the increase in damping produces a smaller resonant response and the shear strain levels correspondingly decrease. When variation in G'' alone is considered (G' constant), the decrease in damping produces a larger resonant response and the shear strain levels are correspondingly seen to increase. When variations in both G' and G'' are considered, the shear strains levels lie somewhere in between.

C. Segmented Treatment

It is well understood that for given modulus and thickness ratios, there exists an optimal length of the constrained layer damping treatment.[16] Because an increase in the length of the treatment beyond the optimal value produces a reduction in damping, this provides a motivation for segmenting the treatment. For configuration 2, the length of the continuous treatment exceeds the optimal length, and the influence of segmentation, as shown in Fig. 11, is examined. Considering linear viscoelastic material behavior only, the damping ratio for the segmented treatment is found to be 8.48% (significantly larger than the 3.78% available with the continuous treatment). Figure 12 compares the shear strain distribution in the viscoelastic layer for the continuous and segmented treatments (considering linear viscoelastic behavior only). For both the continuous and the segmented treatments in Fig. 12, the excitation force amplitude was adjusted so that the peak transverse displacement at resonance was 5% of the beam length. Thus, the spatial distribution of shear strain for the two cases corresponds to identical transverse displacements of the beam. Segmentation clearly produces regions of higher shear strain amplitude at the additional free edges of the treatment, and this is

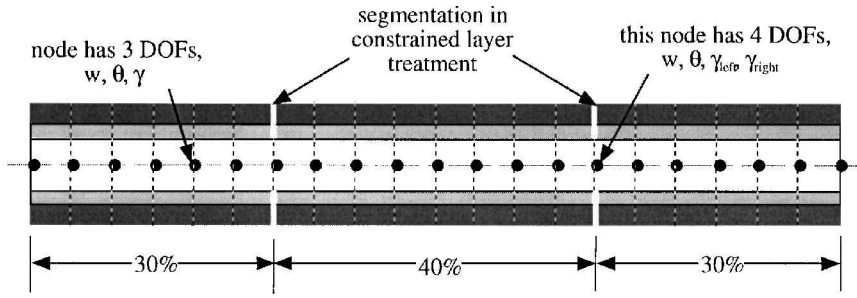

Fig. 11 Finite element discretization of beam with segmented constrained layer damping treatment.

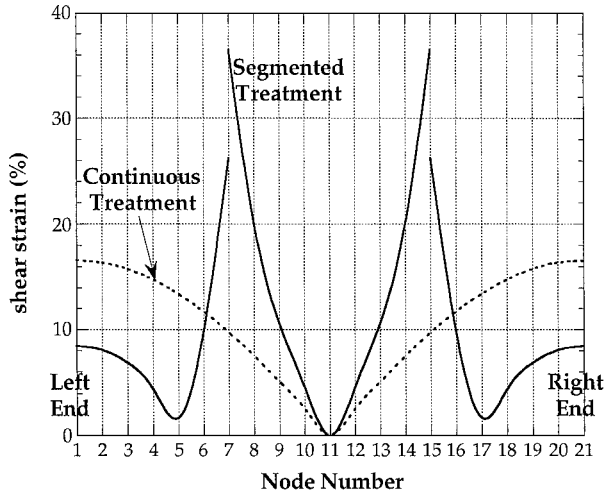

Fig. 12 Variation of shear strain for continuous and segmented treatments.

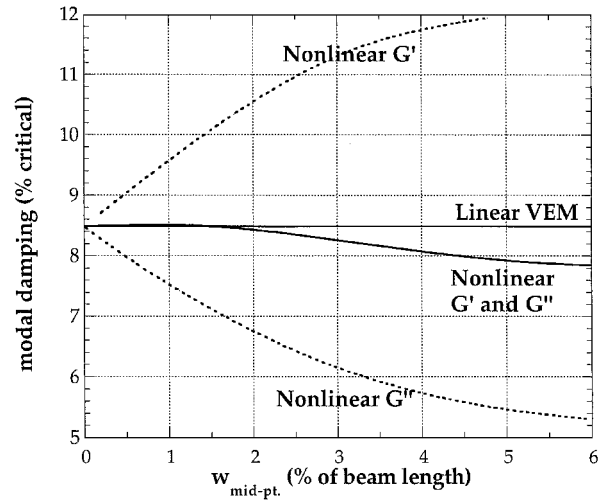

Fig. 13 Modal damping variation as a function of excitation level (segmented treatment).

responsible for the overall increase in damping. When variations in G' and G'' are considered, the variation in damping for increasing excitation levels is shown in Fig. 13. As before, variation in G'' alone (G' constant) reduces the damping, whereas variation in G' alone (G'' constant) increases the damping. The individual influences are almost comparable, with only a slight net decrease in damping when variation in both G' and G'' is considered. A comparison of Figs. 9 and 13 indicates that when the treatment is segmented, the increase in damping due to softening of the viscoelastic layer (variation in G') has a smaller effect. To understand this difference, note that for configuration 2 the viscoelastic layer was very stiff and allowed relatively little shear in the continuous treatment. Segmentation reduced the overall system stiffness considerably (natural frequency reduces from 44.8 Hz for the unsegmented treatment to 32.2 Hz for the segmented treatment). Thus, whereas the softening of the viscoelastic material had a substantial influence on the performance of the unsegmented treatment (which was fundamentally stiff), it had a less significant effect on the performance of the segmented treatment (which was more compliant). If only linear viscoelastic material characterization is considered, a net 4.7% increase in damping ratio is predicted due to segmentation (3.78% for the continuous treatment compared to 8.48% for the segmented treatment). However, if nonlinear viscoelastic material behavior is considered, the increase in damping can be as little as 2.2%. It is conceivable that, for changes in system parameters, an increase in damping due to segmentation may be predicted when linear viscoelatic material characterization is considered, but a decrease in damping may be observed when the nonlinear characterization is considered.

IV. Conclusions

Previous studies on active and passive constrained layer damping treatments have assumed linear viscoelastic behavior. However, many damping materials such as silicone- or carbon-filled elastomers are known to display nonlinear behavior, with the storage and loss modulus generally decreasing with shear strain amplitude. This study examines the influence of such an amplitude-dependent variation of the complex modulus on the performance of a passive constrained layer damping treatment. The observations drawn from the results of the finite element simulations presented are summarized next.

In general, both reduction in storage modulus, as well as loss modulus, with increasing strain amplitude will have an impact on the performance of the damping treatment. The degree of the individual contributions depends on the shear modulus of the viscoelastic material relative to the stiffness of the structure. For increasing excitation levels, the reduction in the loss modulus results in an overall reduction in damping provided by the treatment if the viscoelastic material is relatively compliant. However, if the viscoelastic material is relatively stiff, the reduction in its storage modulus with increasing strain amplitude now allows significantly larger amounts of shear in the layer, and this results in an overall increase in the damping provided by the treatment. The benefits obtained by segmentation of a constrained layer damping treatment could reduce considerably when the nonlinear behavior of the viscoelastic material is considered. This is reasonable because segmentation, in general, increases the shear strain levels in the constrained layer damping treatment, effectively making a relatively stiff damping treatment more compliant.

References

[1] Baz, A., "Active Constrained Layer Damping," *Proceedings of Damping '93*, IBB, San Francisco, pp. 1–23.

[2] Baz, A., and Ro, J., "Optimum Design and Control of Active Constrained Layer Damping," *Transactions of the American Society of Mechanical Engineers*, Special 50th Anniversary Design Issue, Vol. 117B, June 1995, pp. 135–144.

[3] Shen, I. Y., "Hybrid Damping through Intelligent Constrained Layer Treatments," *Journal of Vibration and Acoustics*, Vol. 116, No. 3, 1994, pp. 341–349.

[4]Shen, I. Y., "Bending-Vibration Control of Composite and Isotropic Plates Through Intelligent Constrained Layer Treatments," *Smart Materials and Structures*, Vol. 3, No. 1, 1994, pp. 59–70.

[5]Azvine, B., Tomlinson, G. R., and Wynne, R. J., "Use of Active Constrained-Layer Damping for Controlling Resonant Vibration," *Smart Materials and Structures*, Vol. 4, No. 1, 1995, pp. 1–6.

[6]Huang, S. C., Inman, D. J., and Austin, E. M., "Some Design Considerations for Active and Passive Constrained Layer Damping Treatments," *Smart Materials and Structures*, Vol. 5, No. 3, 1996, pp. 301–313.

[7]Liao, W. H., and Wang, K. W., "On the Analysis of Viscoelastic Materials for Active Constrained Layer Treatments," *Journal of Sound and Vibration*, Vol. 207, No. 3, 1997, pp. 319–334.

[8]Liao, W. H., and Wang, K. W., "On the Active-Passive Hybrid Control Actions of Structures with Active Constrained Layer Treatments," *Journal of Vibration and Acoustics*, Vol. 119, No. 4, 1997, pp. 563–572.

[9]Hausmann, G., "Structural Analysis and Design Considerations of Elastomeric Dampers with Viscoelastic Material Behavior," *Proceedings of the 12th European Rotorcraft Forum*, Garmisch–Partenkirchen, Germany, Sept. 1986.

[10]Felker, F., Lau, B., McLaughlin, S., and Johnson, W. I., "Nonlinear Behavior of an Elastomeric Lag Damper Undergoing Dual Frequency Motion and its Effect on Rotor Dynamics," *Journal of the American Helicopter Society*, Vol. 32, No. 4, 1987, pp. 45–53.

[11]Hausmann, G., and Gergley, P., "Approximate Methods for Thermoviscoelastic Characterization and Analysis of Elastomeric Lead-Lag Dampers," *Proceedings of the 18th European Rotorcraft Forum*, Avignon, France, Sept. 1992.

[12]Gandhi, F., and Chopra, I., "An Analytical Model for a Nonlinear Elastomeric Lag Damper and Its Effects on Aeromechanical Stability in Hover," *Journal of the American Helicopter Society*, Vol. 39, No. 4, 1994, pp. 59–69.

[13]Gandhi, F., and Chopra, I., "A Time-Domain Nonlinear Viscoelastic Damper Model," *Smart Materials and Structures*, Vol. 5, No. 5, 1996, pp. 517–528.

[14]Gandhi, F., and Chopra, I., "Analysis of Bearingless Main Rotor Aeroelasticity Using an Improved Time-Domain Nonlinear Elastomeric Damper Model," *Journal of the American Helicopter Society*, Vol. 41, No. 3, 1996, pp. 267–277.

[15]Thomson, P., Balas, G., and Leo, P., "The Use of Shape Memory Alloys for Passive Structural Damping," *Smart Materials and Structures*, Vol. 4, No. 1, 1995, pp. 36–41.

[16]Plunkett, R., and Lee, C. T., "Length Optimization for Constrained Viscoelastic Layer Damping," *Journal of the Acoustical Society of America*, Vol. 48, No. 1, Pt. 2, 1970, pp. 150–161.

A. M. Baz
Associate Editor